Korean J. Chem. Eng., 38(10), 1983-2002 (2021)
DOI: 10.1007/s11814-021-0865-6

pISSN: 0256-1115
eISSN: 1975-7220

Deep-learning modeling and control optimization framework for intelligent thermal power plants: A practice on superheated steam temperature

Qianchao Wang*, Lei Pan*,†, Kwang Y. Lee, and Zizhan Wu***

*Key Laboratory of Energy Thermal Conversion and Control of Ministry of Education, School of Energy and Environment, Southeast University, Nanjing 210096, China
**Department of Electrical & Computer Engineering, Baylor University, Waco, TX 76798-7356, USA
(*Received 1 February 2021 • Revised 7 June 2021 • Accepted 8 June 2021*)

Abstract−The operational flexibility requirement has brought great challenges to control systems of thermal power plants. Through the big data and deep-learning technology, intelligent thermal power plant can greatly improve the quality of deep peak-load regulation. Based on the framework of an intelligent thermal power plant, this paper proposes a control optimization framework by constructing a hybrid deep-learning simulation model adaptable for multiple disturbances and wide operational range. First, Gaussian naive Bayes is utilized to classify data for identification, in conjunction with prediction error method for fine data extraction. Second, deep long-short term memory is explored to fully learn extracted data attributes and identify the dynamic model. Third, based on the simulation model, two aspects are considered for control optimization: i) For a variety of immeasurable disturbances in thermal processes, the extended state observer is employed for disturbance rejection, and ii) as a widely used heuristic algorithm, particle swarm optimization is applied to optimize the parameters of controllers. Superheated steam temperature (SST) control system is the key system to maintain the safety and efficiency of a power plant; thus the proposed deep learning modeling and control optimization method is applied on the SST system of a 330 MW power plant in Nanjing, China. Simulation results compared with actual data and the index analysis demonstrated the effectiveness and superiority of the proposed method.

Keywords: Gaussian Naive Bayes, Prediction Error Method, Long-short Term Memory, Extended State Observer, Particle Swarm Optimization

INTRODUCTION

Operational flexibility required by the high penetration of renewable energy has brought great challenges to control systems for thermal power plants. Operational flexibility involves fast ramp rate, sufficient power capacity and energy capacity [1] for power units to meet the peak-load regulation requirements from the power grid. Currently, conventional proportional-integral-derivative (PID) control is used in thermal power plants. It is easy to implement and maintain, but it adopts the linearization method, which is not good in dealing with nonlinear dynamics and external disturbances that often result in a flexible operation process [2]. Therefore, it is necessary to improve PID control systems in parameters or strategies for peak-load thermal power units.

The open-loop step-response test for tuning PID parameters is no longer suitable for peak-load thermal power units. A closed-loop simulation model with wide operational range and multiple disturbances becomes necessary for tuning the parameters and optimizing the structure of the control system. Intuitively, the effectiveness of the controller optimization depends on the precision of simulation model. Therefore, this paper proposes an effective high-quality modeling framework by using novel machine-learning methods based on the big-data database that stores all possible operational data of peak-load thermal power units, which serves as a modeling tool for closed-loop control optimization simulation system.

In this paper, two aspects are considered for improving the accuracy of the model. The first is data extraction. In industrial processes, system identification is affected by external interferences, and sometimes special manipulation or manual operation, which may break the closed-loop identifiable condition and cause inevitable identification error. For obtaining a high-precision model, the identification data must meet the conditions for closed-loop identification of a large inertia process to achieve sufficient informatization [3]. To estimate the parameters of the thermal plant the input signal must be persistently excited. Therefore, the input and output of each plant must be under continuous dynamic changes in significant amount so that the dynamic characteristics of thermal processes can be manifested. Therefore, digging for identifiable data is the first important step for model identification. There are many studies on data-mining for fault diagnosis [4], decision-making analysis [5], communication network [6] and so on, but little on digging the closed-loop identifiable data. To mine the best identifying data from big-data samples, Gaussian Naive Bayes (GNB) classifier is used in conjunction with prediction error method (PEM) to form a two-step classifier.

Actually, as a powerful classifier, Naive Bayesian can effectively mine data to learn the relationship between attributes, which has been fully utilized and developed in many aspects of life, for instance, for improving the precision of meteorological data mining [7], analyzing driver injury severity in rear-end crashes [8], micro-blog topic

†To whom correspondence should be addressed.
E-mail: panlei@seu.edu.cn

tracking [9], and improving network security performance [10]. As a popular probabilistic method, it also has been widely used in industry. Adedipe, Shafiee and Zio [11] reviewed and evaluated existing work on Bayesian network model in the field of wind energy. They found that the use of Bayesian networks in the wind energy industry is very broad, which includes wind power and weather forecasting, fault diagnosis and prognosis. Marlis, et al. [12] proposed a new implementation of the GNB classifier for classification in all searchlights and demonstrated its advantage compared to other more complex classifiers. Based on these observations, this paper studied the GNB data classifier for screening the closed-loop identifiable data from the big data.

Another aspect of model identification is accuracy. PEM adopts the maximum likelihood theorem to estimate model parameters to reduce the error continuously between the model output and the actual data. PEM has been widely used and various optimized PEMs have been proposed. Relatively simple PEM based on non-stationary predictors that are linear in the outputs is presented by Abdalmoaty and Hjalmarsson [13] to solve the estimation problem for stochastic parametric nonlinear dynamic models. Aiming to model nonlinear and unstable target system, Maruta and Sugie [14] also proposed a stabilized PEM. Currently, data-driven practices mainly involve black-box modeling, fault diagnosis, etc., in power plants, but rarely involve data extraction before modeling. Therefore, a data extraction method based on massive data resources is proposed uniting GNB classifier and PEM to improve the quality of identification model, where GNB classifier can preliminarily extract data and PEM can set thresholds to further extract identifiable data.

Another aspect to improve modeling accuracy is considering a deep-learning method. In theory, neural networks can approximate arbitrary nonlinear models by fully learning the attributes from data. With the deepening of the neural network depth, the model accuracy will get better. Considering that industrial data are all time-series from dynamic systems, recurrent neural networks (RNN) are often adopted as dynamic models [15]. However, due to the complex structure of the traditional RNN, sometimes with the increase of the network depth the problem of gradient disappearance and explosion will gradually limit the development of the network [16]. To circumvent this problem, long short-term memory (LSTM) has emerged. It can be superimposed on other types of neural networks to solve different problems. For instance, convolutional long short-term memory (Conv-LSTM) has been developed to identify diabetes from the clinical and physical data [17] to address the human action recognition issue [18]. Besides, some new types of LSTM have been applied to industrial prediction and modeling. An aggregated LSTM model was proposed by Haoran et al. [19] to predict air pollution effectively and accurately. A nonlinear voltage prediction algorithm based on LSTM with model construction was presented by Chen [20] to predict deformation mirror voltages. Considering its strong capability to describe nonlinear dynamic characteristics and stable computational performance based on python, this paper adopts a deep LSTM (DLSTM) modeling method to carry out the modeling after data extraction, resulting in GNB-PEM-DLSTM for short.

Based on the resulting accurate model with the GNB-PEM-DLSTM, the aim of optimizing control strategy and parameters can be achieved based on the closed-loop control system. It is highly convincing to verify the optimization results by comparing the simulation with actual data because of the high fidelity of modeling. This deep-learning modeling and control optimization method conforms to the idea of intelligent control of a thermal power plant with the prospect of broad application. Fig. 1 shows an overall scheme of an intelligent thermal power plant. Relying on the big-data storage platform, a large number of power plant data can be stored in the platform according to different delivery strategies, which can be analyzed in different aspects using big-data analytic methods. For different control purposes, the results of data analysis can be used on different control modules. The proposed deep-learning modeling and control optimization method in this paper can be integrated into the artificial intelligence (AI) deep-learning assemble and improve the actual control process. By control optimization, the controllers of thermal power plants can be further updated with new actual data acquired. According to the new data entering into the big-data storage platform, new dynamic characteristics of models can be learned further for control strategy optimization.

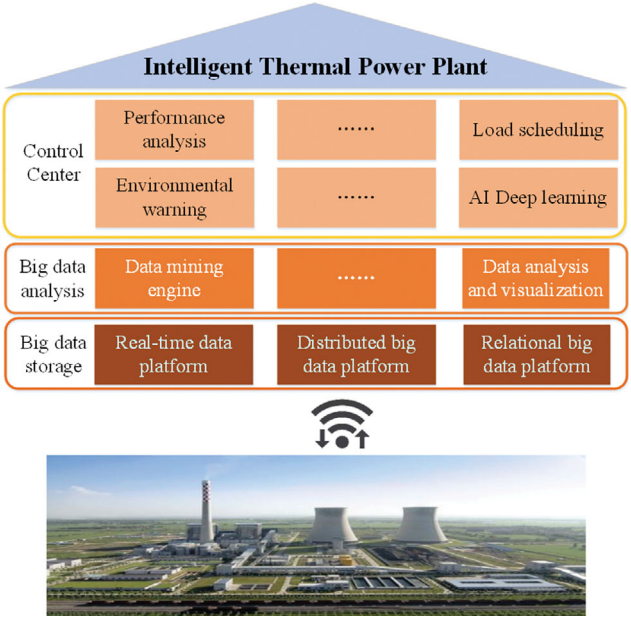

Fig. 1. Interaction between the simulation system and the power plant monitoring system.

As a main component of a boiler, the superheated steam temperature (SST) control system needs special attention among the multiple control systems. SST is located at the last stage of the steam-water flow path where there is much disturbance from the gas side of heat-exchangers and has the dynamics of large inertia, time-varying parameters, and nonlinearity, which are difficult for conventional PID to handle [21]. Some advanced control strategies have been proposed to solve the above problems, e.g., the multi-objective optimization (MOO) algorithm with conflicting objectives [22], neuro-PID controller [23] and active disturbance rejection control (ADRC) [24] for SST improvement, and the basic fuzzy control for high-pressure SST in a once-through boiler [25]. These works

optimize the control strategy of SST from various angles to improve the control performance.

In this paper, the cascaded PID control of superheater in a thermal power plant in Nanjing, China, is taken as the object of study, where the PID optimal control is studied from two aspects. First, an extended state observer (ESO) is augmented to the original PID control system to improve the disturbance-rejection performance. The SST system has several unknown disturbances, such as electricity or heat load changes, boiler soot blowing, changes of coal types, and so on. The ESO can estimate the disturbance and compensate for it in real time based on the input and output data. In industrial process control, many people have combined other control methods to study the anti-interference ability of the ESO. Chen et al. [26] developed a fuzzy ESO according to the stable fuzzy predictive control which has been validated on a power plant model. To improve the control performance for power level in a nuclear power plant, Hui et al. [27] proposed an ESO based adaptive dynamic sliding mode control scheme. Improved ESO combined with other controller can also be applied for frequency control of wind power [28] and wide range load tracking without being affected by unknown disturbances [29].

Secondly, the PID parameters need to be retuned after the augmentation of ESO since it usually changes the system characteristics. Data-driven closed-loop parameter optimization is adopted based on the convenience of the big-data platform. The PID parameters optimized with actual data including disturbances are more practical than the parameters set by the open-loop tuning. In power systems, particle swarm optimization (PSO) is used for various purposes, such as optimizing the economic dispatching of the electric power systems [30], performance evaluation of turbo-generator subsystem [31], determining the optimal allocation of distributed generators to reduce the total active and reactive losses and voltage regulations of the network [32], and the optimization of the design and operating conditions of post combustion CO2 capture (PCC) [33]. The PSO can also optimize parameters of other algorithms to achieve the goal of the corresponding algorithms, for example, power load prediction [34]. Therefore, PSO is used in this paper for PID parameter optimization in order to achieve the ideal control performance when the ESO-augmented PID control system is put into automation.

With the requirement of operational flexibility on peak-load thermal power units, good control performance of the SST is essential for maintaining device safety and the plant efficiency. To strictly control the SST, this paper considers the deep-learning approach and utilizes the big-data resource to develop more valid modeling and control optimization approaches on the SST, which can be integrated into the intelligent power plant. The following are the main contributions of this paper:

(1) This paper proposes an advanced data extraction method for the united Gaussian Naive Bayes classifier and the PEM for establishing an accurate model of the SST system.

(2) Advanced deep neural network, LSTM, is used to establish the model. By fully learning the extracted data attributes, the LSTM can accurately reflect the model's dynamic characteristics and achieve quality control.

(3) The PSO is employed to optimize parameters in the inner- and outer-loop of PID, and the add-on ESO controller is designed for disturbance rejection.

The structure of the proposed strategy is shown in Fig. 2. First, the field data and historical data are sent in GNB-PEM for extraction. Second, before identification, the extracted data is normalized and then the DLSTM is utilized to identify the model. Third, the proposed control optimizations such as ESO-PID, PSO-PID and ESO-PSO-PID are utilized searching for better performance and

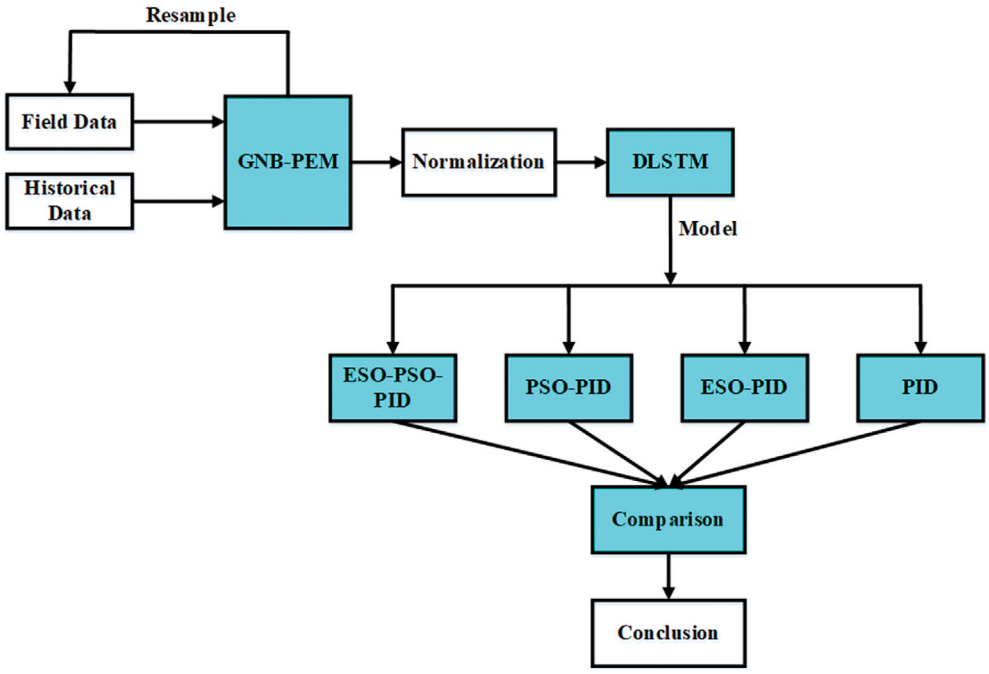

Fig. 2. The structure of the proposed modeling and control optimization strategy.

then their control performances are compared among the controllers.

The rest of the paper is organized as follows. A deep-learning modeling method is introduced in Section 2. In Section 3, an accurate SST model is identified and compared with the linear model, and the accuracy of identified model is verified and control optimizations are carried out. On the basis of simulation, the advanced control strategies of the SST control system are evaluated with comparison in Section 4, and conclusions are drawn in Section 5.

DEEP-LEARNING MODELING

Deep learning involves data extraction and modeling. In this section, a hybrid of Gaussian Naive Bayesian (GNB) and prediction error method (PEM) for data extraction is presented first and then a deep long short-term memory (LSTM) neural network is presented for modeling.

1. Data Extraction Approach

Because real industrial data contains many influencing factors, such as variable operating conditions of equipment, random interferences, measurement noise and so on, it is necessary to extract a data segment that meets the model identification requirements through a data extraction approach. Therefore, in this paper, a statistical method, called GNB-PEM data extraction approach, is proposed to effectively extract the massive data to improve modeling accuracy. The flowchart of the GNB-PEM extraction approach is shown in Fig. 3.

The brief steps of the GNB-PEM data extraction method are presented as follows:

(1) In the preliminary screening, the identifiable data is made into a training set, and the on-site data is also made into a testing set after variable selections.

(2) The classifier is trained according to the principle of Gauss Naive Bayes, and the test set is preliminarily classified.

(3) Based on the PEM rapid model construction and the model fitting threshold, data can be extracted in detail.

(4) If the data does not fit the requirement for modeling, new data are sampled.

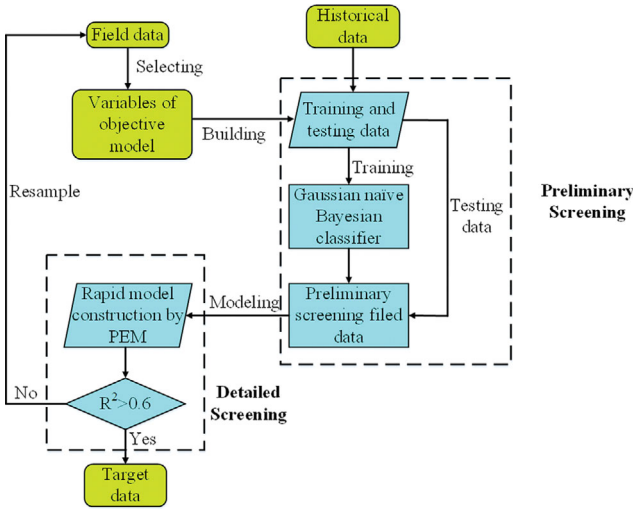

Fig. 3. The flow chart of GNB-PEM.

1-1. Preliminary Extraction of Data Based on GNB Classifier

Power plant desuperheater data is made of a number of attributes, such as the inlet steam temperature, the valve opening and the total steam flow. Data for each attribute can be categorized into two categories: recognizable data and difficult-to-recognize data. Then the Naive Bayesian classification can be expressed as follows. When the category is certain, the conditional independence between attributes is shown as:

$$P(a|x)=\frac{P(a)P(x|a)}{P(x)}=\frac{P(a)}{P(x)}\prod_{i=1}^{d}P(x_i|a) \tag{1}$$

where x is a set of attributes of the plant to be identified, a is the categories of attributes, P(a) and P(x|a) are, respectively, the prior probability and conditional probability; P(x) is probability of attributes which is the same for all categories; d is the number of attributes. To estimate P(a|x), both P(x|a) and P(a) need to be calculated based on the training data.

Assuming that all the attributes are independent of each other, the Naive Bayesian probability P_{nb} of all categories is calculated by comparing the maximum probability and its corresponding category, which is shown as:

$$P_{nb}(x)=\text{argmax}P(a)\prod_{i=1}^{d}P(x_i|a) \tag{2}$$

When the power plant operates near the nominal operating point, the data distribution of superheated steam temperature can be approximately Gaussian distribution. Therefore, the conditional probability will be shown as:

$$P(x_i|a)=\frac{1}{\sqrt{2\pi\sigma_a^2}}e^{-\frac{(x_i-\mu_a)^2}{2\sigma_a^2}} \tag{3}$$

where μ_a and σ_a^2 are both under category a; μ_a is the mean of x; σ_a^2 is the variance.

1-2. Detailed Extraction of Data Based on PEM

The prediction error method (PEM) is a widely used identification method [12]. Parameter θ of the model is adjusted to reach the minimum root mean squared error. The prediction error model is defined as:

$$z(t)=f[z(t-1),\ldots,z(1),z(0),u(t-1),\ldots,u(1),u(0),\theta]+e(t,\theta) \tag{4}$$

where u(t) and z(t) are, respectively, the input and output vectors at time t; e(t, θ) is the prediction error.

According to the above model, e(t, θ) is minimized and the best model is selected. To achieve the purpose, $D_N(\theta)$ is used as a cost function which is associated with the covariance matrix of e(t, θ):

$$D_N(\theta)=\frac{1}{N-m+1}\sum_{k=m}^{N}e(t,\theta)e^T(t,\theta) \tag{5}$$

where m and N are, respectively, the beginning and end of the data.

The estimation criteria are usually in the following two forms:

$$J_N^1(\theta)=\text{tr}[RD(\theta)] \tag{6}$$

$$J_N^2(\theta)=\log[\det D(\theta)] \tag{7}$$

where R is a positive definite matrix.

Generally, to minimize $J_N^1(\theta)$ or $J_N^2(\theta)$, a nonlinear steady-state

system model parameter estimation technique, such as gradient method, is usually adopted.

According to the above principle, PEM can be used for modeling without overly considering the accuracy of the model. By setting a reasonable model fitting threshold, it can be used to further extract the preliminarily extracted data.

R-Squared (R^2) principle is a commonly used indicator to determine the degree of model fit. Since it eliminates the influence of dimensions, it is better than other indicators, such as MSE, MAE, and RMSE. Based on the R-Squared principle [35], the fitting threshold is shown to be:

$$R^2 = 1 - \frac{\Sigma \|z - \hat{z}\|_2}{\Sigma \|z - \bar{z}\|_2} \tag{8}$$

where z, $\hat{z}$ and $\bar{z}$ are, respectively, the actual output, the simulated output and the mean of actual output.

2. Deep Long Short-Term Memory for Modeling

After the data extraction, the modeling method for nonlinear dynamic system is further considered. Deep-neural networks are a multi-layer neural network that can fit nonlinearity well. Considering that the data from industrial processes is always time series from dynamic systems, long short-term memory (LSTM) neural network is applied for model construction in this paper, which is better than the traditional fully connected RNN, whose output at time k is calculated by the unit state at time k−1 and the input at time k.

The LSTM is an improved RNN model, learning long-term information to solve the gradient vanishing and explosion problem. It introduces the concept of gate, which differs from the traditional RNN. The gate can reduce the interference of the new information to the existing information so as to achieve the long-term storage effect of information of modules. The specific description of LSTM is introduced in Appendix A.

MODELING OF SUPERHEATED STEAM TEMPERATURE CONTROL SYSTEM

The SST control system of a 330 MW thermal power unit in Nanjing, China, was modeled based on the pre-data extraction and deep-learning modeling method for control optimization in this section.

1. Variable Selection of SST System

In the SST system, the steam is desuperheated by the desuper-

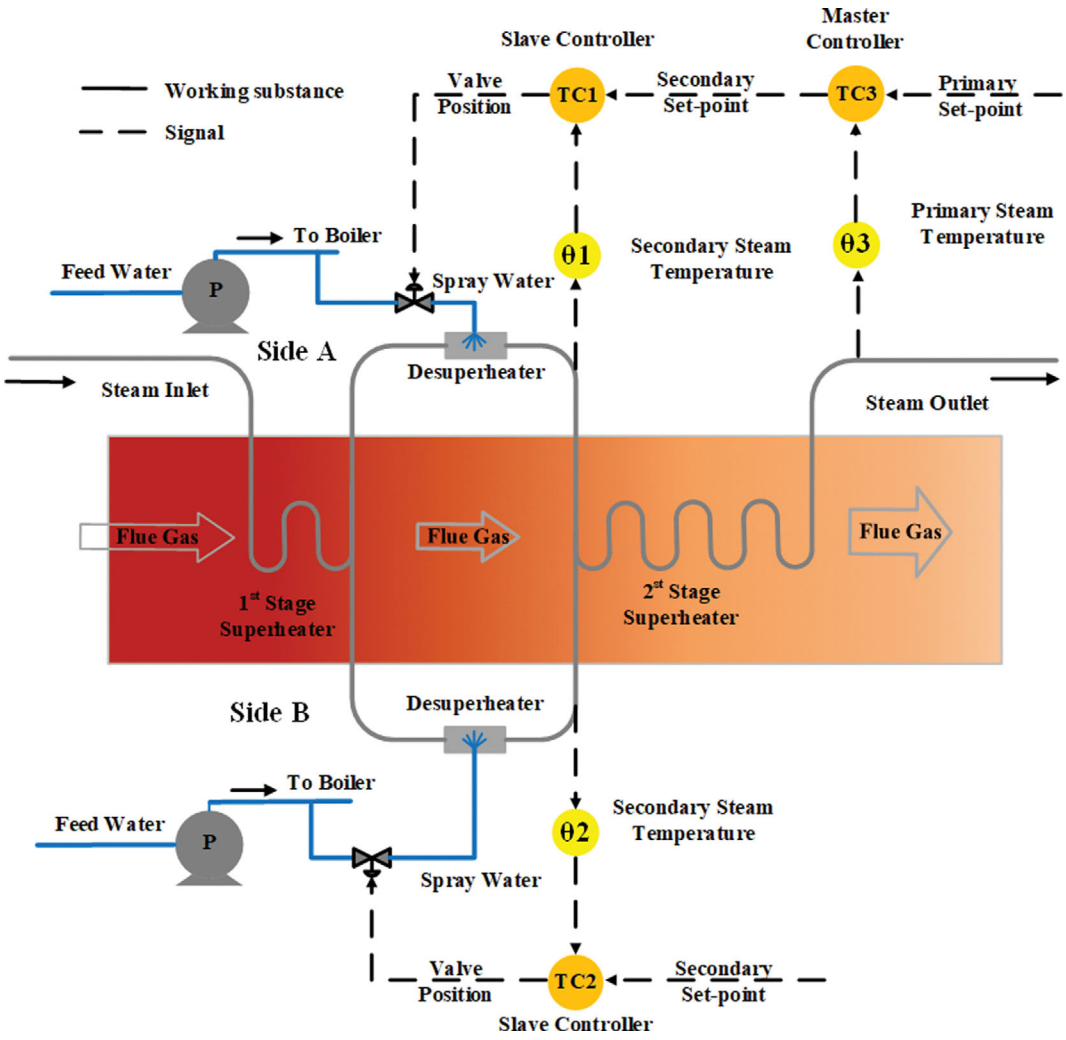

Fig. 4. Schematic diagram of the secondary SST control system.

heating water and then heated by the secondary superheater. The general temperature of secondary superheated steam is controlled by secondary desuperheating water within 540±5 °C.

The secondary SST control system, shown in Fig. 4, has two desuperheaters and one superheater, and cascaded PID control strategy is applied for controlling. The steam temperature is desuperheated to $\theta 1$ and $\theta 2$, and then heated to $\theta 3$, in °C. Furthermore, the actual water leakage of the desuperheating water valve at Side A is much more than that of the valve at Side B in this specific thermal power unit.

From a comprehensive analysis from thermodynamics and correlations among variables, the inputs of the two desuperheaters are the desuperheater inlet steam temperature (°C), total steam flow (t/h) and valve opening of desuperheating water (%), denoted either as u_{a1}, u_{a2}, u_{a3} or u_{b1}, u_{b2}, u_{b3}. The output of the two desuperheaters is the outlet steam temperature (°C) of desuperheaters, denoted as y_a or y_b. The input of the secondary superheater is the inlet temperature of secondary superheater of Sides A and B (°C) and steam flow of Sides A and B (t/h), which are denoted as u_1, u_2, u_3 and u_4. The outlet temperature of secondary superheater (°C) is the output denoted as y.

For closed-loop identification of a thermal power generating plant, a long time relative steady-state data around 950t/h steam is generated for the modeling. The sampling time is 1 second, with 17,608 groups of data. When there is a large change in the total steam flow, the valve opening and the steam temperature of the desuperheaters vary greatly. Located at the rear of the flue gas passage, the secondary SST is affected by unknown disturbances and always has strong fluctuations.

2. GNB-PEM Classification

From the historical data, only a small amount of data can be used for the identification of the secondary SST. By data analysis, the categories of attributes are two, divided into (i) recognizable data and (ii) difficult-to-recognize data, and the P(a) in Equation (1) is calculated with historical data and found to be 1/10, which is the probability of the recognizable data distribution. According to P(a), the training set can be composed of 10,000 recognizable data and 90,000 difficult-to-recognize data. The new field data is chosen as the testing set. The label of identifiable sample is set to 1 and the unidentifiable sample is set to 2.

The GNB classifier is tested by testing set, and the two following identifiable data segments are extracted and shown in Appendix B.

There are some differences between Fig. B1 and Fig. B2, which means the dynamic characteristics of the two data segments are different. In Fig. B1, the amount of flow has a steady increase in the beginning and a sharp decrease after that. But in Fig. B2, most of the time, the flow stays at the same level around 940t/h and shows an upward trend at the end. The valve openings at Side A and Side B are around 7% and 20%, respectively, but the fluctuation of the valve opening is obvious. With the fluctuation of valve opening, input steam temperature of desuperheater and the steam flow, the other variables fluctuate, reflecting the characteristics of the system. Overall, both data segments meet the requirements of identification.

According to Eq. (8), the threshold of model fit is set to 60%. Based on PEM and the two extracted identifiable data segments, two linear models of the two desuperheaters at Sides A and B are built rapidly. After comparing the fit of the two models with the threshold, the 100-10,100th group of data is obtained as the best data segment for identification.

The identified linear desuperheater models at Sides A and B and the secondary superheater model are, respectively, shown below:

$$y_a = \frac{0.0051}{z-0.9910}u_{a1} + \frac{-3.799\times10^{-4}}{z-0.9910}u_{a2} + \frac{-0.0085}{z-0.9910}u_{a3} \quad (9a)$$

$$y_b = \frac{0.0037}{z-0.9947}u_{b1} + \frac{-1.929\times10^{-6}}{z-0.9947}u_{b2} + \frac{-0.0025}{z-0.9947}u_{b3} \quad (9b)$$

$$y = \frac{0.0011}{z-0.9963}u_1 + \frac{0.0119}{z-0.9963}u_2 + \frac{1.3\times10^{-4}}{z-0.9963}u_3 + \frac{5.598*10^{-5}}{z-0.9963}u_4 \quad (10)$$

where the variables are as defined in Section 3.1, i.e., u_{a1}, u_{a2}, and u_{a3} (or u_{b1}, u_{b2}, and u_{b3}) are, respectively, the desuperheaters' inlet steam temperature (°C), total steam flow (t/h), and valve opening of desuperheating spray water (%) on Side A (or Side B); y_a or y_b are the outlet steam temperature (°C) of desuperheaters on Side A or Side B, and y is the outlet temperature of the secondary superheater (°C).

3. Model Construction by Deep LSTM Aided with Thermodynamic Calculation

The closed-loop system of the SST can be simulated based on the dynamic model identified from the obtained identifiable data and the actual power plant control strategy. However, since there is only a total steam flow measurement on the head for the two desuperheaters in the power plant, it cannot be used in modeling both sides of the desuperheater satisfactorily. Therefore, a thermodynamic calculation is used for estimating the absent steam flow split on both sides.

3-1. Thermodynamic Calculation for Absent Measurement Points

By analyzing the dynamic characteristics of the secondary SST system in Fig. 5, the steam flow of Sides A and B denoted as u_3 and u_4 can be estimated accurately.

According to the measured steam temperature t_1, t_3 and steam pressure p_1, p_3, respectively, at the inlet and outlet of desuperheater, and the temperature t_2 and pressure p_2 of the desuperheating water, the corresponding enthalpy H_1, H_2, H_3 can be calculated. Based on energy conservation theory, an equation can be established for the

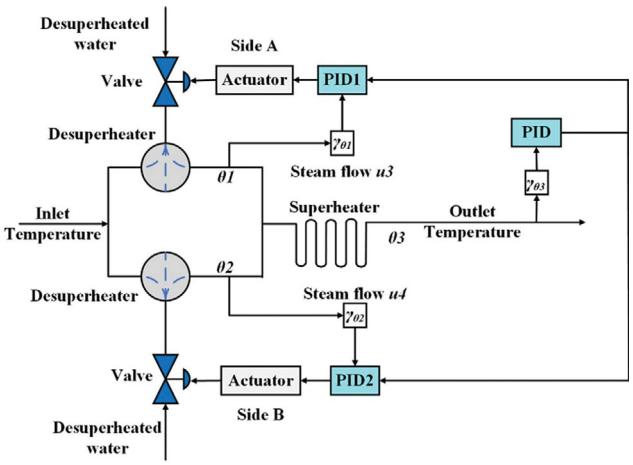

Fig. 5. Schematic diagram of the secondary SST control system.

thermodynamic systems of desuperheaters at Sides A and B as shown below:

$$F_L(H_3-H_1)=F_P(H_3-H_2) \tag{11}$$

where F_L is the steam flow at Side A or B; H_3 and H_1 are, respectively, the enthalpy of the steam at the outlet and inlet of desuperheater; F_P is the spray flow at Side A or B; H_2 is the enthalpy of spray water.

According to formula (11), the steam flow on Sides A and B, denoted as F_{LA} and F_{LB}, can be roughly estimated. Then, according to the measured total steam flow F, the estimated steam flows at Sides A and B are further adjusted by

$$F_{Li}=\frac{F_{Li}}{F_{LA}+F_{LB}}F \tag{12}$$

where i is A or B; F is the total steam flow.

At last, the calculated steam flow is shown in Fig. 6.

As can be seen in Fig. 6, because the amount of total steam flow is certain, the characteristics of steam flow at Side A and B are opposite. As the steam flow at Side A increases, the steam flow at Side B decreases. The amount of steam flow at Side A is around 425t/h, which is lower than Side B, around 519t/h. The steam flow at both sides has sufficient fluctuation.

3-2. Modeling by Deep LSTM

Based on the principle of LSTM and the data extracted by the GNB-PEM, three models are established, respectively, for Sides A and B desuperheaters and the secondary superheater. Five-fold verification method is applied in this paper.

Before training the deep LSTM, normalization of data is necessary. Normalization can unify evaluation standards and avoid unnecessary numerical problems. The data normalization is shown by:

$$x_i=\frac{x_i-\bar{x}_i}{\sigma_i} \quad i=1\sim n \tag{13}$$

where x_i is the *i*-th feature of input variables, and σ_i is the variance of x_i.

In the structure of the deep LSTM in this paper, the input and output layers have three neurons and one neuron, respectively. Twenty-five neurons are in the three gates, respectively, as the hidden layers. The biases of the three gates are random numbers. There are four layers in the deep LSTM.

After training, three models are validated through validation sets. The fit reaches 75%. The output of the model is introduced in Appendix C.

From Fig. C1, the volatility of simulated data of all three identified models is consistent with the actual data. The biases between field data and simulation are acceptable. Therefore, in this paper, the GNB-PEM extraction method is feasible and the calculation of the steam flow at Sides A and B is reasonable.

3-3. Comparison between PEM and LSTM Models

The open-loop simulation on the PEM model and LSTM model was performed and the inputs of models are the actual desuperheater valve openings. The outlet steam temperature of desuperheater at Sides A and B and secondary superheater is, respectively, shown in Fig. 7.

From Fig. 7(c), some differences can be observed between the output temperature of PEM model and LSTM model. There is around an 80 s delay in the PEM response compared to the set point, which is difficult to support the reasonable design of controllers. However, the LSTM response does not have a delay. Especially, from 5,300 s to 7,000 s, even though the errors between LSTM and actual data are larger, which may be caused by some unknown disturbance or the steep change of set point, the trend of LSTM is consistent with actual data because of having no delay compared with PEM. As a simulation platform for improving control performance, the consistency with actual data on the trend is more important than accuracy. Furthermore, the superheated steam temperature response by PEM has a steep drop at around 2,700 s, which did not happen in the actual data. Moreover, the response of PEM fluctuates more than the LSTM response. In general, the deep

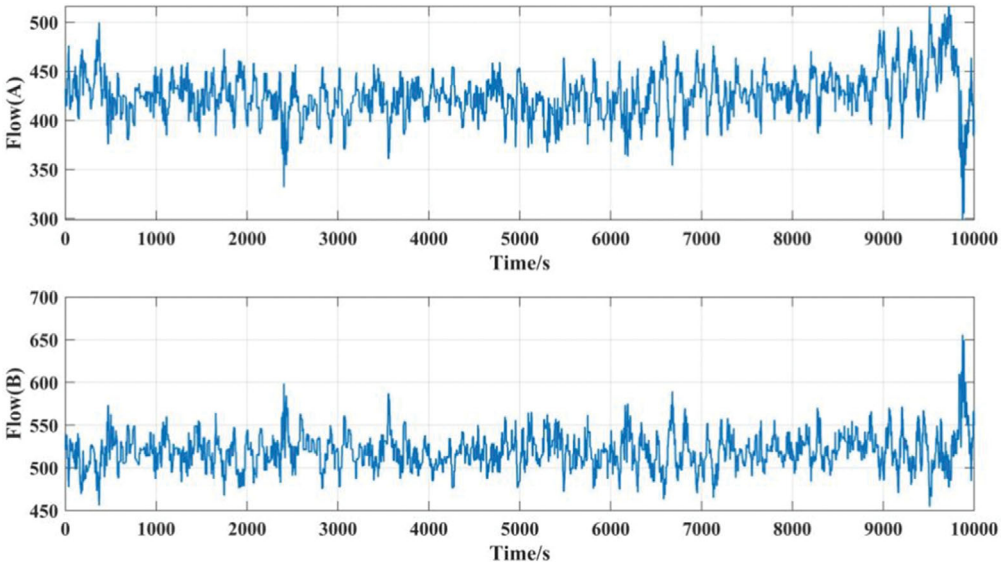

Fig. 6. Steam flow at Sides A and B.

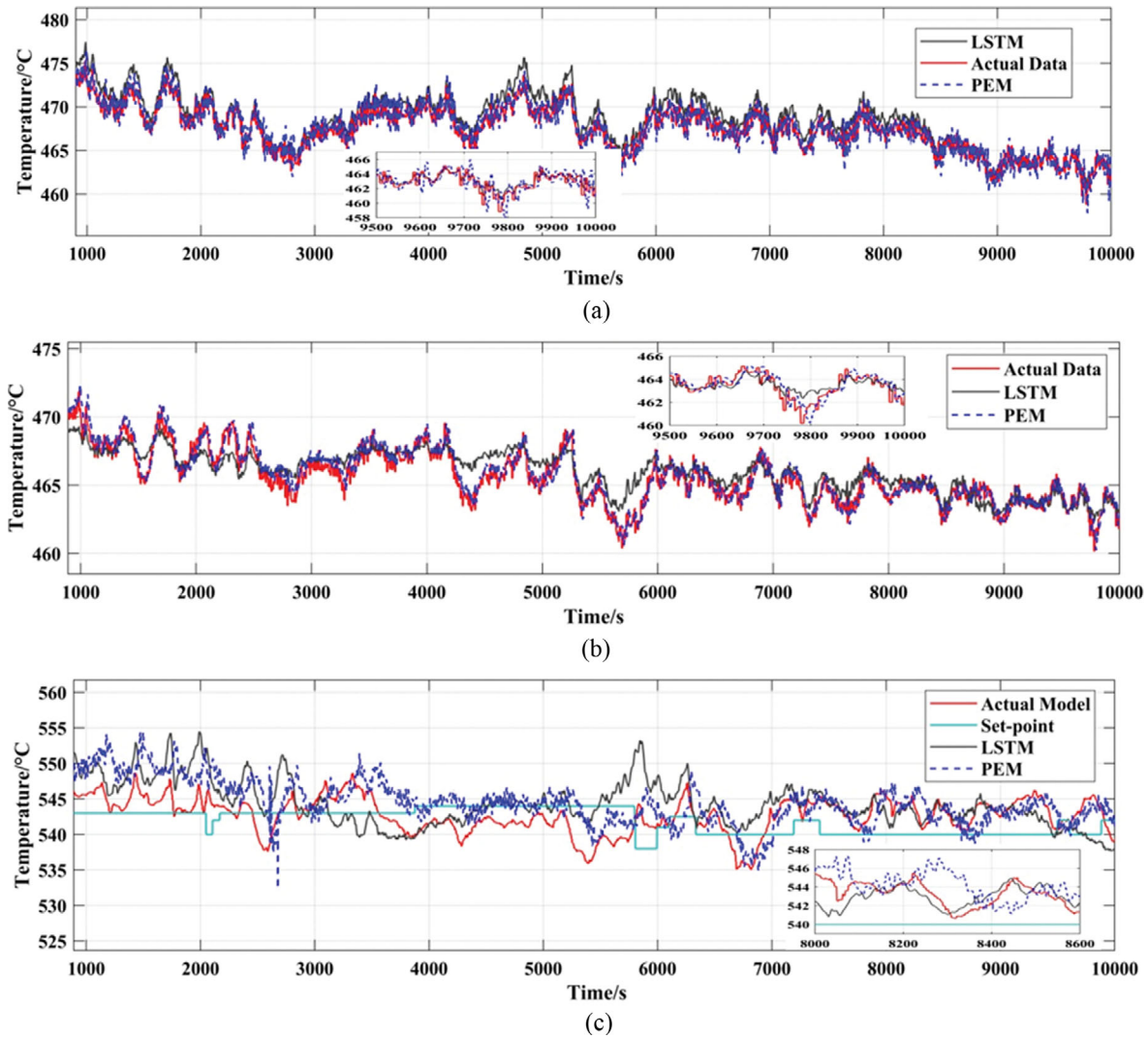

Fig. 7. Comparison between PEM and LSTM models. (a) Outlet steam temperature of desuperheater at Side A. (b) Outlet steam temperature of desuperheater at Side B. (c) Outlet steam temperature of secondary superheater.

LSTM model is better than the PEM model in responding to nonlinearity.

3-4. Closed-loop Simulation Verification

According to the actual control system of the power plant, the control strategy of SST system is cascaded PID control which is shown in Fig. 5. The PID control parameters of outer loop are k_p=0.6, k_i=0.0005. And the PID control parameters of inner loop of Sides A and B are k_{pa}=2.4, k_{ia}=0.004, k_{pb}=2.5, k_{ib}=0.0083. The set-point of the SST is set manually. The simulation results are shown in Fig. 8.

As can be seen from Fig. 8, although the secondary superheated steam temperature has some magnitude error with respect to the real data, the fluctuation pattern is the same and the valve openings at Sides A and B are consistent with the actual opening. In general, the GNB-PEM extraction method and the LSTM identified model are feasible approaches for obtaining an accurate model. However, to improve the precision of SST, the control strategy needs to be improved.

OPTIMIZATION ON CONTROL SYSTEM

The operational flexibility required by the high penetration of renewable energy has brought great challenges to control systems of thermal power plants. However, traditional PID control can no longer meet this requirement. In this paper, the improvement on PID control system on SST is made by two different approaches. The first one is adding an ESO without affecting the original PID controller. The second one is optimizing PID parameters by improved PSO.

1. Active Disturbance Rejection Control

In Fig. 8, the PID cascaded controller only controls the valve openings of the desuperheaters. So, the steam flow at each stage and the inlet steam temperature of desuperheaters can be considered as disturbances in improving the stability of the SST and valve openings. An active disturbance rejection control (ADRC) can be used in this model. The specific principle description is introduced in Appendix D.

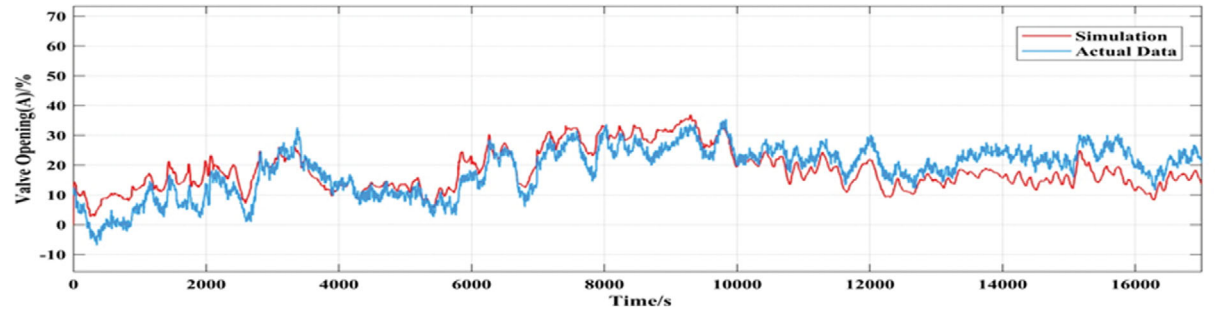

(a)

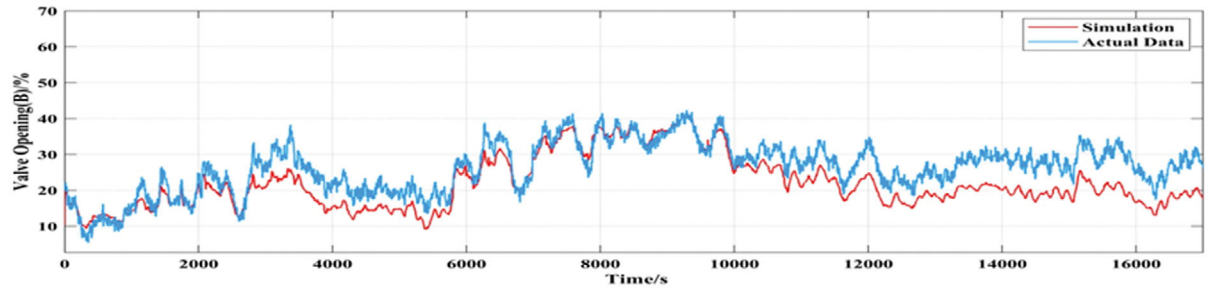

(b)

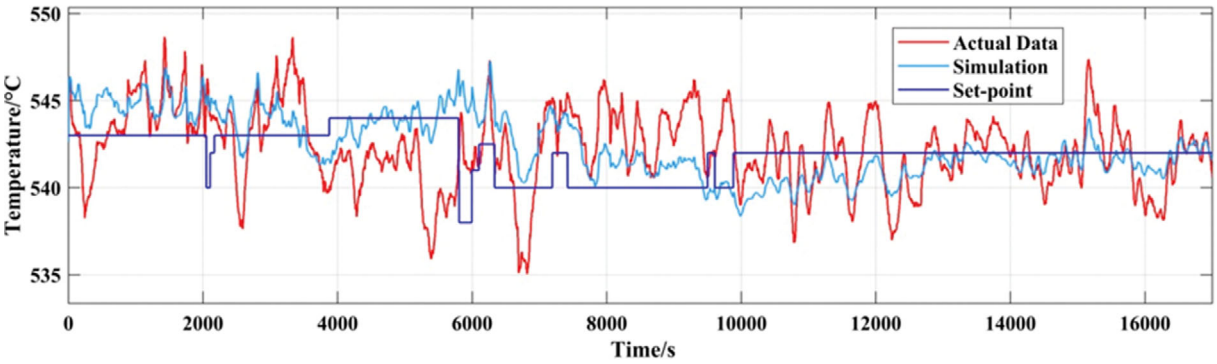

(c)

Fig. 8. Closed-loop simulation. (a) Valve opening of Side A. (b) Valve opening of Side B. (c) Outlet steam temperature of secondary superheater.

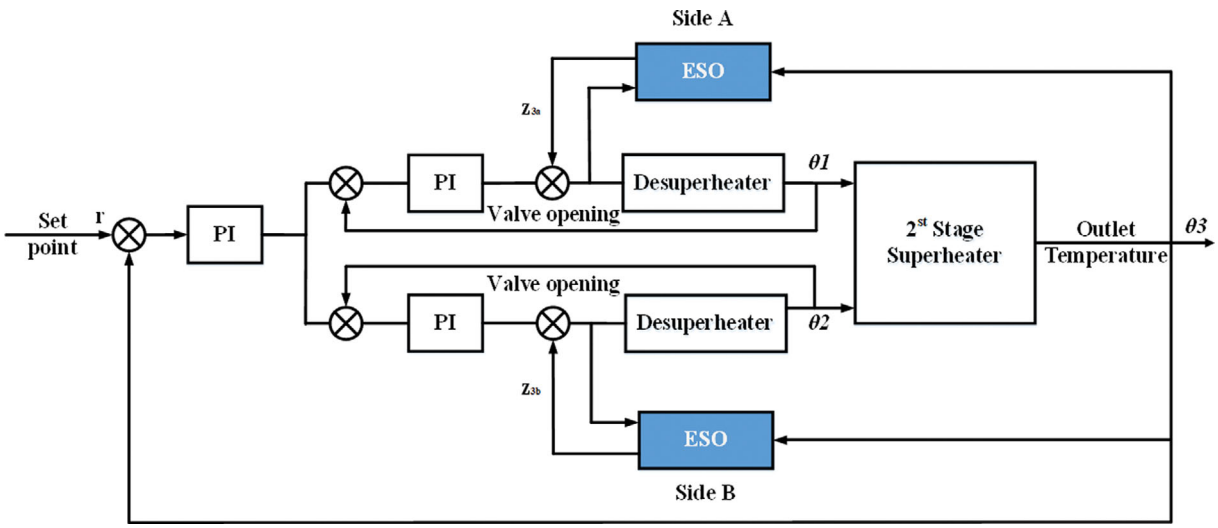

Fig. 9. The closed-loop simulation based on ESO.

From Fig. 5, it can be seen that when other inputs, including the inlet steam temperature of desuperheaters and the steam flow, are viewed as disturbances, the system can be considered as two models with few disturbances connected in parallel. The ADRC is established based on the above principle and the closed-loop simulation model is shown in Fig. 9.

Because the calculated steam flow and the measured inlet steam temperature of the desuperheater are not much different on Sides A and B, to reduce the design difficulty the ESO parameters of Sides A and B are designed to be the same. The parameters of ESO can be set to w_0=5, b_0=0.5. According to actual parameters, PID are set to k_p=0.6, k_i=0.0005, k_{pa}=2.4, k_{ia}=0.004, k_{pb}=2.5, k_{ib}=0.0083. The simulation results are shown in Fig. 10.

The tracking effect is more obvious when the disturbance is large as shown in Fig. 10(c). The anti-interference effect of the ADRC is mainly reflected in the disturbance of steam temperature. Compared with PID control, the steam temperature under ADRC has less fluctuation when there is a sudden disturbance. However, the whole fluctuation of the steam temperature still remains and is basically the same as that under PID control. This may be caused by the deviation of the parameters of the PID, so it is important to explore the optimal parameters of PID.

1-1. Frequency Domain Analysis on Control System

A closed-loop transfer function is essential for system analysis in frequency domain. Considering the difficulty of analytical description of the closed-loop system with LSTM model, this paper conducts frequency domain analysis on the linear model identified by PEM whose response is consistent with that of the deep LSTM as was shown in Fig. 7 as an approximation. The derivation of the closed-loop transfer function of the superheated steam temperature is given below.

Based on (D.3) and (D.5) and taking the Laplace transform, z_3 can be obtained as:

$$z_3 = -\frac{w_0^2}{(s-4w_0)(s+w_0)}(s^2 y - b_0 u) \tag{14}$$

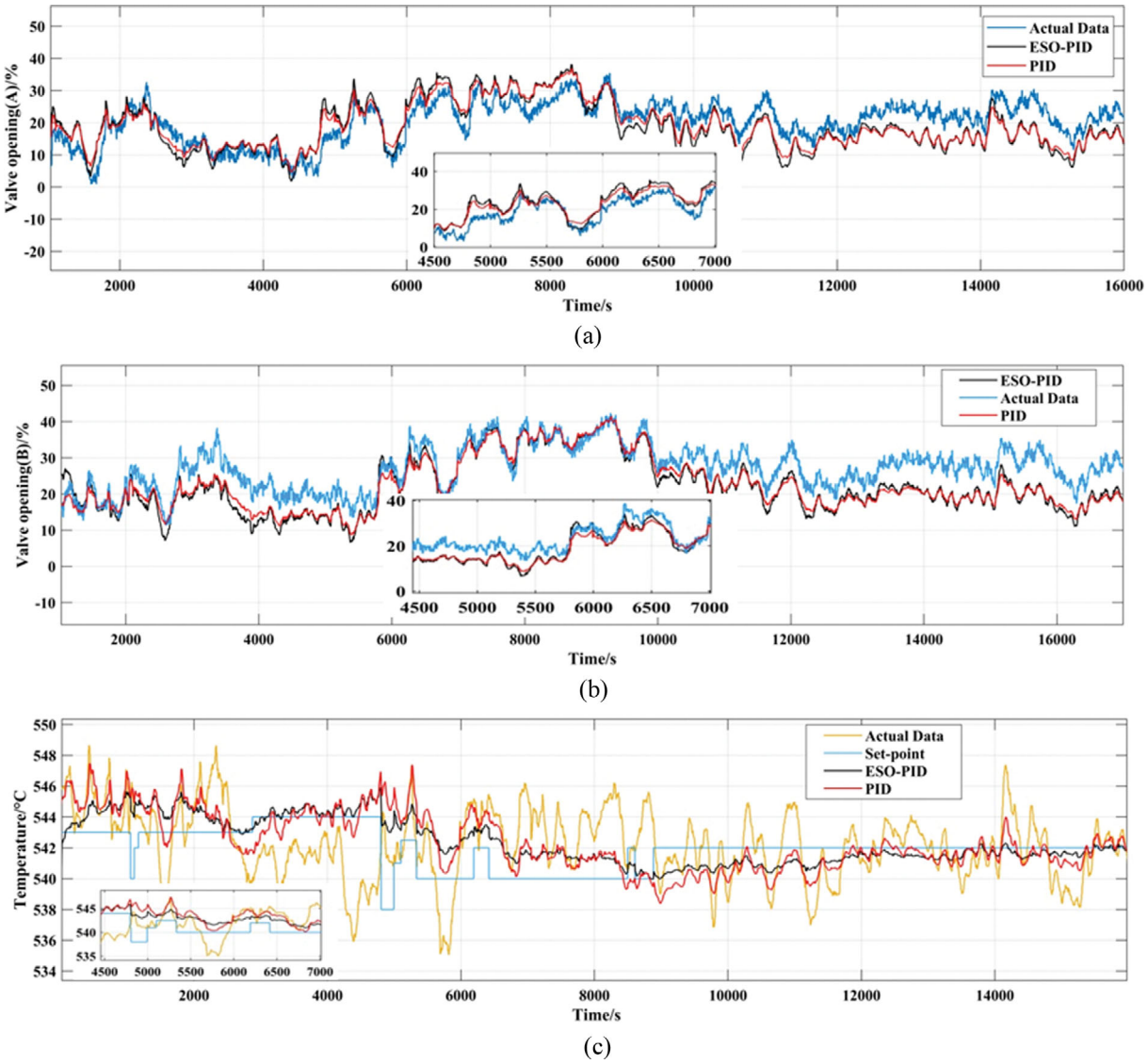

Fig. 10. ADRC simulation. (a) Valve opening of Side A. (b) Valve opening of Side B. (c) Outlet steam temperature of secondary superheater.

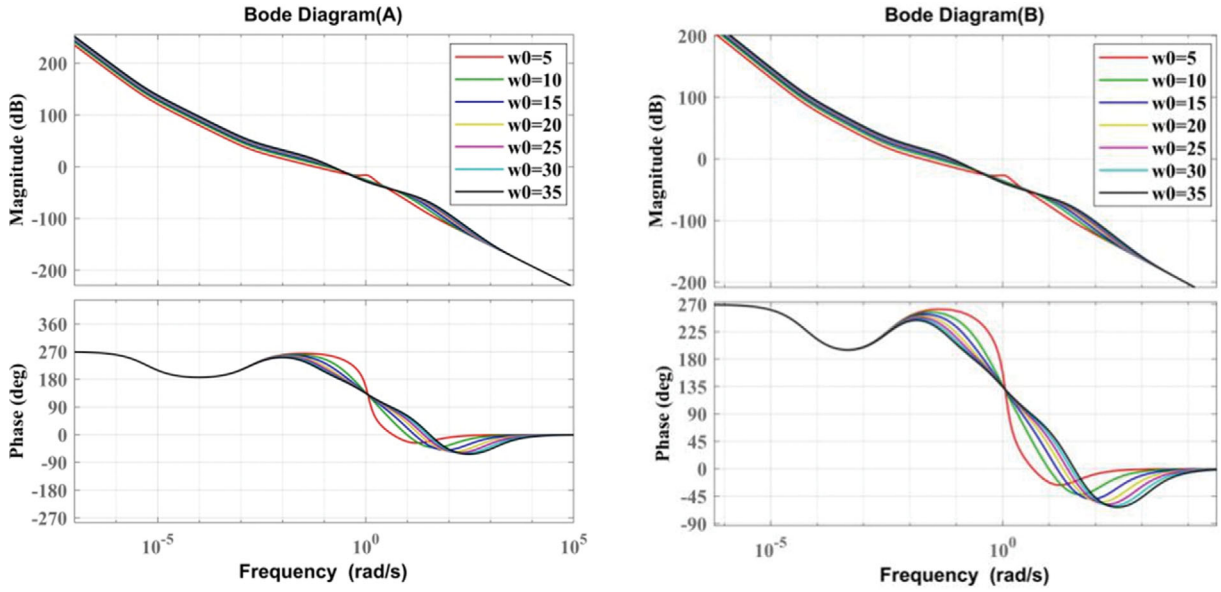

Fig. 11. Bode diagram of the closed-loop system, for (a) Side A, and (b) Side B.

According to the transfer functions of linear models (9)-(10) and Fig. 9, the whole model containing two desuperheaters and one superheater can be split into two parallel models for Side A and B. In each parallel model, input is the desuperheaters' inlet steam temperature and output is the superheaters' outlet steam temperature. Each model is a 2-nd order linear model with transfer function described as:

$$G(s)=\frac{b}{s^2+a_1s+a_2} \tag{15}$$

Based on Fig. 9, after simplifying the controlled object and the control loop composed of ESO, we can obtain the internal model structure of ESO [39] and the structural transformation of ADRC which is shown in Appendix E.

Based on the internal model structure, Fig. 11 shows the effect of the bandwidth changes at Sides A and B observers on the system. The bandwidth w_0 is set to 5, 10, 15, 20, 25, 30 and 35. With the increase of w_0, Table 1 shows the phase margins and cut-off frequencies of the closed-loop system.

It can be seen from the table and figures that with the increase of w_0, the cut-off frequency of the system gradually increases, which results in faster response speed. However, the phase margin and stability of the system is reduced. Hence, w_0 is related to the estimation accuracy of ESO.

Table 1. Cut-off frequency and phase margin with different w_0

w_0	Cut-off frequency (rad/s)		Phase margin (/°)	
	A	B	A	B
5	0.0620	0.0134	443.28	438.73
10	0.1145	0.0355	422.37	436.57
15	0.1434	0.0507	401.37	426.20
20	0.1553	0.0604	388.78	415.75
25	0.1587	0.0734	380.34	405.34
30	0.1599	0.0797	375.56	397.70
35	0.1631	0.0831	371.48	391.37

2. Optimization of PID Controller Parameters

The SST PID control system controls the temperature of superheated steam with two desuperheater control valves, one on Side A and another on Side B. The characteristics of a desuperheater control valve are affected by not only variables of desuperheaters but also the valve at the other side.

There are two more reasons for giving valve opening an importance. First, valve opening characteristics represent the control action as one of the indicators of control performance. Under the premise of ensuring the stability of superheated steam temperature, the fluctuation of valve opening should be as small as possible for keeping the unit thermal efficiency. Second, different control systems have different valve characteristics. By comparing the characteristics of the valves, we can know the control effect of PSO-PID, ESO-PID and ESO-PSO-PID controllers on the valves. Finally, by comparing the control performance of both valves and superheated steam temperature, a better controller can be determined.

As time passes, the factors that affect the parameters of the SST system are constantly changing, such as changes in coal type, aging of equipment, or increased corrosion. Therefore, to obtain a better control performance, experienced staff tends to be more inclined to manual control in actual operation of the power plant. However, this is not in line with the development trend of intelligent power plants. Therefore, it is necessary to further optimize the PID parameters under the premise of automatic control. Heuristic optimization algorithms have been widely used in many production processes. As a commonly used heuristic optimization algorithm, PSO has been considered for its fast convergence speed and efficiency.

In this paper, PSO is used to optimize the PID parameters in

order to make the SST more stable and track the set point closely. The original PID parameters of the plant are selected as the initial values of the PSO algorithm. The initial population is 30 and the maximum iteration is 15. The speed of particles is limited to [−1, 1]. The cost function of PSO is improved by considering the volatility of the valve and the integral of time multiplied by the absolute error criterion (ITAE) in the cost function instead of a single ITAE to select suitable parameters and reduce local optimization. The PSO parameter optimization process is as follows:

(1) Optimize the PID parameters of inner loop of Sides A and B. Initialize parameters of PSO.

(2) Calculate the fitness of each particle in the population and update the optimal position of particles.

(3) Update the velocity and position of particles.

(4) After the maximum number of iterations is reached, output the PID parameters corresponding to the global optimal position.

(5) Repeat the above four steps to optimize the PID parameters of the outer loop.

After optimization, the PID parameters are k_p=0.4704, k_i=0.00762, k_{pa}=3.3332, k_{ia}=0.3263, k_{pb}=8.9382 and k_{ib}=0.4080. The simulation is shown in Fig. 12, where ESO-PID refers to the disturbance rejection by ESO based on PID control, PSO-PID refers to the PID controller optimized by PSO and ESO-PSO-PID refers to the disturbance rejection by ESO based on optimized PID control.

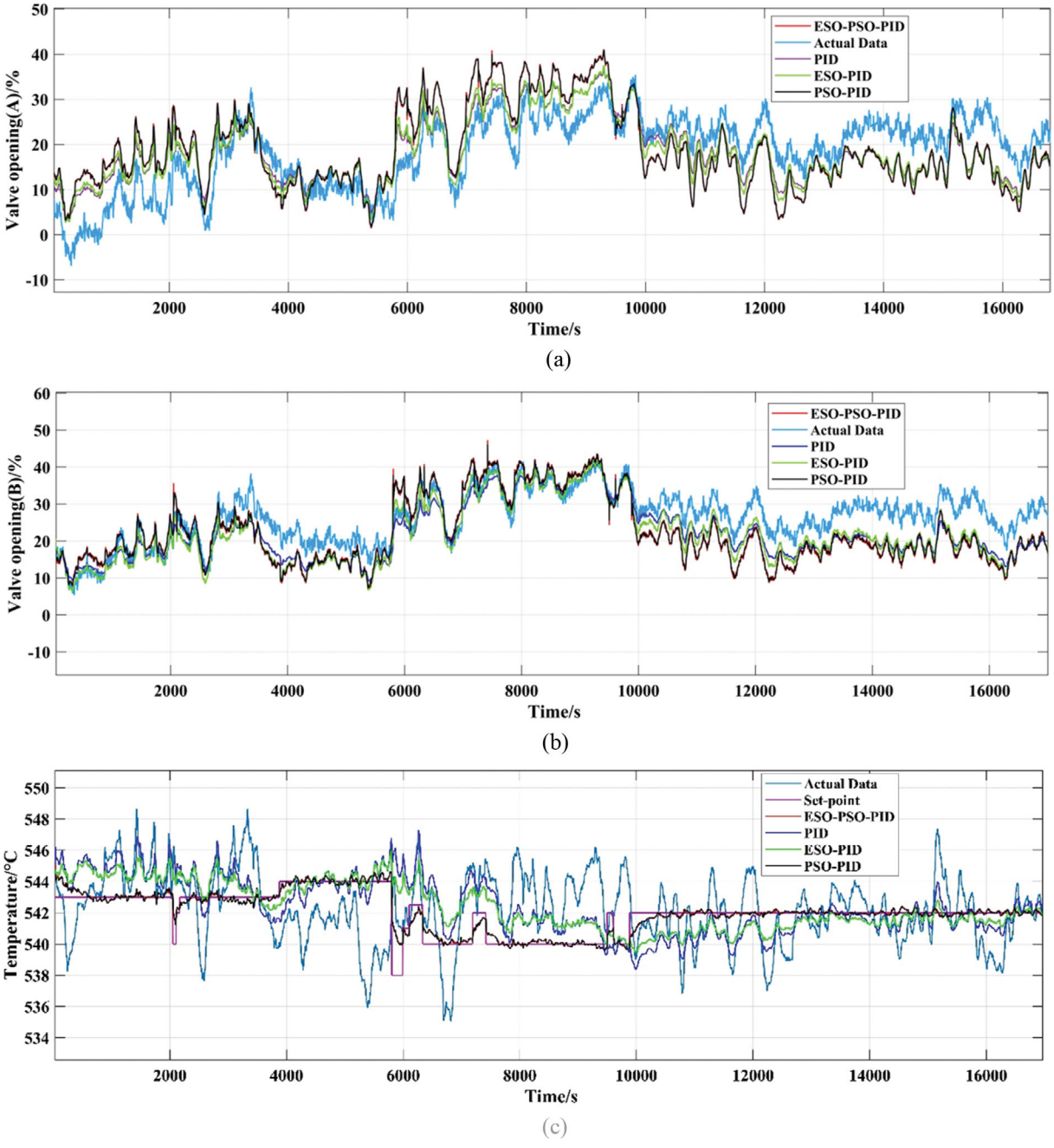

Fig. 12. PSO-PID simulation. (a) Valve opening of Side A. (b) Valve opening of Side B. (c) Outlet superheated steam temperature.

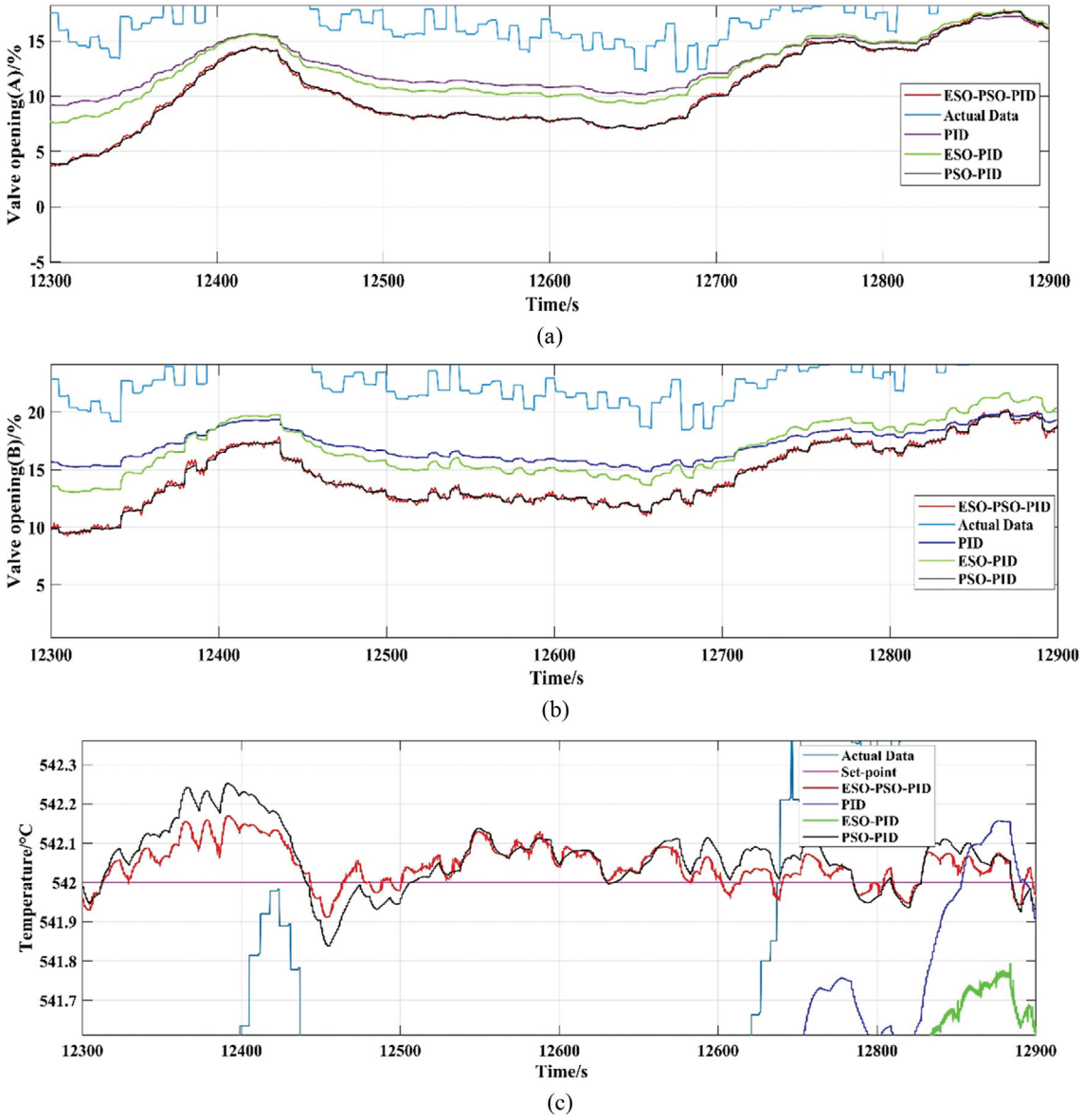

Fig. 13. Zoomed PSO-PID simulation. (a) Valve opening of Side A. (b) Valve opening of Side B. (c) Outlet superheated steam temperature.

According to the parameters optimized by PSO, the control performance of outlet superheated steam temperature has been greatly improved. The steam temperature can track the set-point tightly. Besides, the fluctuation of valve opening is in a reasonable range. Therefore, the optimization of PID parameters is extremely important for control performance.

There is hardly any significant overshoot in the control performance of PSO-PID and ESO-PSO-PID. At around 10,000 s, when the set-point has increased to 542 °C, the outlet superheated steam temperature controlled by PSO-PID and ESO-PSO-PID can increase faster to follow the set-point than PID and ESO-PID. The settling time of PSO-PID and ESO-PSO-PID is around 478 s, which is much lower than 3,480 s, the settling time of ESO-PID and the PID.

In Fig. 12, the control performances of PSO-PID and ESO-PSO-PID seem to be similar over the large time range. To examine more closely, the figures are zoomed in over a short time range, 12,300 s-12,900 s, as shown in Fig. 13.

According to Fig. 13(c), the control performance of PSO-PID and ESO-PSO-PID is much better than that of ESO-PID and single PID. Furthermore, the error between the set-point and the control performance of ESO-PSO-PID is smaller than PSO-PID. Overall, the control performance of ESO-PSO-PID is the best. When the valve openings between the two controllers are not very different, the superheated steam controlled by ESO-PSO-PID is closer to the set-point. For further study, the following three kinds of analysis strategies are performed.

3. R-Squared and MSE Analysis

The R-squared (R^2) fitting threshold (8) can describe the degree of correlation of two variables. In order to be able to compare the degree of fit between the SST and the set-point, the field data z in R^2 in (8) is replaced by the set-point. Considering that the model of the secondary SST control system has several inputs, the following

Table 2. R^2_adjusted and MSE of four control methods

Controller	R^2_adjusted	MSE
PID	0.398	6.55
PSO-PID	0.895	3.403
ESO-PID	0.423	6.175
ESO-PSO-PID	0.898	3.399

adjusted R^2 [40] is adopted in this paper for more accurate judgment:

$$R^2\_adjusted = 1 - \frac{(1-R^2)(n-1)}{n-p-1} \tag{16}$$

where p is the number of attributes, and n is the number of samples.

Besides R^2, MSE is also a commonly used control performance indicator which can be defined as:

$$J = \frac{1}{m}\sum_{i=1}^{m}(y_m - \hat{y}_m)^2 \tag{17}$$

where y_m is set value and $\hat{y}_m$ is the simulation result. The R^2_adjusted and MSE of the three control methods are shown in Table 2.

According to the performance index of MSE, the performance of the outlet steam temperature under the ESO-PSO-PID controller is much better than the other three controllers. Adding an ESO without tuning original PID controller can improve the control effect to a certain extent. However, the PID parameters are the key factor for the control effect.

4. ITAE Analysis

The ITAE criterion is the minimum criterion of integral of time multiplied by the absolute error e(t), which can be expressed as:

$$J = \int_1^{\infty} t|e(t)|dt \tag{18}$$

Because valve opening has no set-point, the ITAE cannot reflect the characteristics of the valve opening. To effectively reflect the fluctuation of the valve opening and compare the advantages and disadvantages of the three control methods, this paper integrates the valve opening fluctuations based on the idea of ITAE as

$$J = \int_2^{\infty} t|u(t) - u(t-1)|dt \tag{19}$$

where u(t) is the valve opening.

For the above three control methods, corresponding performance indices are calculated as shown in Table 3.

As can be seen from Table 3, the performance indices of valve openings and outlet steam temperature of secondary superheater are the best under the ESO-PSO-PID controller. The ESO-PID can reject the disturbance within a certain range, and the performance of outlet steam temperature is improved over the initial PID. Nevertheless, the valve openings have more fluctuations, which makes the valves switch more frequently. The control performance of PSO-PID is similar to ESO-PSO-PID. In general, to achieve the most ideal control performance, tuning of the PID parameters must be emphasized in all optimizations.

In summary, the comparison of the four PID controllers in Tables 2 and 3 shows that the control performance of ESO-PSO-PID has the highest R^2_adjusted, the least MSE, and the least ITAE, which means it is better than other three PID controllers.

CONCLUSION

In order to be able to absorb more renewable energy and improve the flexibility of thermal power generating units, the SST needs to be accurately modeled and controlled at a reasonable interval at all times. To tackle the problem, this paper first combines the GNB classifier and PEM to extract the closed-loop data of SST. Then, the optimizations are considered in two aspects in order to fully control the SST and valve openings. First, an extended state observer (ESO) is augmented to the original PID control system to improve the disturbance-rejection performance. Second, the PID parameters are retuned by PSO after the augmentation of ESO since it usually changes the system characteristics. From the simulation results the following conclusions are drawn: i) GNB-PEM can effectively extract actual data for modeling, ii) Deep LSTM can fully learn the extracted data attributes and reflect the dynamic characteristics of the model to establish an accurate model, iii) ESO can effectively reject disturbances caused by dynamic changes in set points, and iv) PSO can effectively search for the optimal PID parameters for better control performance. The simulation results show that the SST fluctuations become smaller and the disturbance is significantly reduced. In general, the proposed GNB-PEM-DLSTM can be used in an SST control system to extract the field data and model the SST dynamics. The PID parameters searched by PSO can improve the control performance significantly, and the resulting intelligent power plant would be an important future power plant development.

Because of the limited data amount, the model cannot contain all disturbances, for example, the disturbance from the flue gas or combustion section. To solve it, our study will continue improving the model construction and the control strategy. One is to study further in big data technology and deep-learning method for more accurate data and models, another is to develop more advanced

Table 3. Improved ITAE of four control methods

Controller	Valve opening at Side A	Valve opening at Side B	Outlet steam temperature of secondary superheater
PID	364.2420	330.1069	3.5672e^04
PSO-PID	168.4789	220.3153	6.6138e^03
ESO-PID	440.1732	480.5423	3.0975e^04
ESO-PSO-PID	167.986	220.1256	6.5986e^03

control method to overcome the influence of unmodeled disturbance to the whole system.

ACKNOWLEDGEMENTS

This work was supported by the National Natural Science Foundation of China under Grants 51576040 and 51936003. The authors would like to give our sincere appreciation to the editor and anonymous referees for their careful review and valuable suggestions.

AUTHOR CONTRIBUTIONS

Qianchao Wang: Methodology, Software, Validation, Data curation, Writing - original draft, Visualization. Lei Pan: Methodology, Formal analysis, Investigation, Resources, Writing - original draft, Supervision, Project administration. Kwang Y. Lee: Resources, Writing, Analysis. Zizhan Wu: Programming, Writing.

CONFLICTS OF INTEREST

The authors declare no conflict of interest.

REFERENCES

1. R. F Nielsen, N. Nazemzadehm, L. W. Sillesen, M. Andersson, K. Gernaey and S. S. Mansouri, *Comput. Chem. Eng.*, **140**, 106916 (2020).
2. A. M. Najar and D. K. Arif, *J. Phys.: Conference Series*, **1218**, 012055 (2019).
3. C. Fang and D. Xiao, *Process identification*, Tsinghua University Press, Beijing (1988).
4. S. Zheng and J. Zhao, *Comput. Chem. Eng.*, **135**, 106755 (2020).
5. Y. Guo, N. Wang, Z. Xu and K. Wu, *Mechanical Syst. Signal Process.*, **142**, 106630 (2020).
6. Q. Zheng, Y. F. Li and J. Cao, *Comput. Commun.*, **163**, 84 (2020).
7. Y. Zhang and J. Sun, *2nd International conference on electrical, computer engineering and electronics*, 996-1001 (2015).
8. C. Chen, G. Zhang, R. Tarefder, J. Ma, H. Wei and H. Guan, *Accident Anal. Prevention*, **80**, 76 (2015).
9. J. Feng, X. He and P. Wang, *Comput. Digital Eng.*, **45**, 2244 (2017).
10. Y. Nuo, *Int. J. Appl. Dec. Sci.*, **11**, 1 (2018).
11. T. Adedipe, M. Shafiee and E. Zio, *Reliability Eng. Syst. Saf.*, **202**, 107053 (2020).
12. O. O. Marlis, L. C. Agustin, V. Giancarlo, G. Rainer and V. S. Mitchell, *NeuroImage*, **163**, 471 (2017).
13. M. R. Abdalmoaty and H. Hjalmarsson, *Automatica*, **105**, 49 (2019).
14. I. Maruta and T. Sugie, *IFAC-PapersOnLine*, **51**, 479 (2018).
15. W. Yu, I. Y. Kim, and C. Mechefske, *Mechanical Syst. Signal Process.*, **149**, 107322 (2021).
16. G. Rao, W. Huang, Z. Feng, and Q. Cong, *Neurocomputing*, **308**, 49 (2018).
17. M. Rahman, D. Islam, R. J. Mukti, and I. Saha, *Computational Biol. Chem.*, **88**, 107329 (2020).
18. Z. Zhang, Z. Lv, C. Gan and Q. Zhu, *Neurocomputing*, **410**, 304 (2020).
19. H. R. Yan, Y. Qin, S. Xiang and H. Chen, *Measurement*, **165**, 108205 (2020).
20. Y. Chen, *Optik*, **220**, 164869 (2020).
21. H. Fan, Z. Su, P. Wang and K. Y. Lee, *Appl. Therm. Eng.*, **170**, 114912 (2020).
22. H. Fu, L. Pan, Y. Xue, L. Sun, D. Li, K. Y. Lee, Z. Wu, T. He and S. Zheng, *IFAC-PapersOnLine*, **50**, 3227 (2017).
23. J. Zhang, F. Zhang, M. Ren, G. Hou and F. Fang, *ISA Trans.*, **51**, 778 (2012).
24. F. L. Xiao, J. H. Zhang, D. Y. Zhu and C. Zhang, *IFAC Proceedings Volumes*, **34**, 505 (2001).
25. T. Nahlovsky, *Procedia Eng.*, **100**, 1547 (2015).
26. C. Chen, L. Pan, S. Liu, L. Sun and K. Y. Lee, *Sustainability*, **10**, 4824 (2018).
27. J. Hui, S. Ge, J. Ling and J. Yuan, *Annals Nuclear Energy*, **143**, 107417 (2020).
28. C. Chen, K. Zhang, K. Yuan and W Wang, *IFAC-PapersOnLine*, **50**, 4388 (2017).
29. F. Zhang, X. Wu and J. Shen, *Appl. Therm. Eng.*, **118**, 90 (2017).
30. G. Yuan and W. Yang, *Energy*, **183**, 926 (2019).
31. H. P. Jagtap, A. K. Bewoor, R. Kumar, M. H. Ahmadi and L. Chen, *Reliability Eng. Syst. Saf.*, **204**, 107130 (2020).
32. H. M. Pesaran, M. Nazari-Heris, B. Mohammadi-Ivatloo and H. Seyedi, *Energy*, **209**, 118218 (2020).
33. H. Xi, P. Liao and X. Wu, *Appl. Therm. Eng.*, **184**, 116287 (2021).
34. W. Song, C. Cattani and C. H. Chi, *Energy*, **194**, 116847 (2020).
35. A. Gelman, B. Goodrich, J. Gabry and A. Vehtari, *The American Statistician*, **73**, 307 (2019).
36. L. Sun, D. Li, K. Hu, K. Y. Lee and F. Pan, *Ind. Eng. Chem. Res.*, **55**, 6686 (2016).
37. K. J. Åström and T. Hägglund, *Advanced PID control*, International society of automation, Pittsburgh (2006).
38. D. Tang, Z. Gao and X. Zhang, *Control Theory & Applications*, **34**, 101 (2017).
39. Q. Xu, M. Sun, Z. Chen and D. Zhang, *In Proceedings of the 32nd Chinese Control Conference*, 5408 (2013).
40. O. Hard, *J. Appl. Statistics*, **36**, 1109 (2009).

APPENDIX A.

The structures of a traditional RNN and the LSTM modules are shown in Fig. A1.

The unit state C_{t-1} and the output h_{t-1} transmitted from time t−1 and the input X_t at time t constitute the input data of LSTM module. The output is the unit state C_t and the output h_t at time t.

Three kinds of gate structures are contained in each neural module: input gate i_t, forgetting gate f_t, and output gate o_t. The input gate i_t determines how much input X_t is reserved in C_t, the forgetting gate f_t determines the influence of C_{t-1} on C_t, and the output gate o_t determines how much state unit C_t remains in the output h_t. Then C_t and h_t are involved in the calculation of LSTM at time t+1.

The calculation of LSTM module is given as following:

$$\text{Forgetting gate:} \quad f_t=\text{sigmoid}(W_f[h_{t-1}, x_t]+b_f) \tag{A1}$$

$$\text{Input gate:} \quad i_t=\text{sigmoid}(W_i[h_{t-1}, x_t]+b_i) \tag{A2}$$

$$\text{Unit state:} \quad c_t=f_t c_{t-1}=i_t \tanh(W_c[h_{t-1}, x_t]+b_c) \tag{A3}$$

$$\text{Output gate:} \quad o_t=\text{sigmoid}(W_o[h_{t-1}, x_t]+b_o) \tag{A4}$$

$$\text{Output:} \quad h_t=o_t \tanh(c_t) \tag{A5}$$

where W and b are respectively the weight and the bias of the three gates.

Sigmoid and tanh are activation functions of LSTM, as defined below:

$$\text{sigmoid}(x)=\frac{1}{1+e^{-x}} \tag{A6}$$

$$\tanh(x)=\frac{e^{x}-e^{-x}}{e^{x}+e^{-x}} \tag{A7}$$

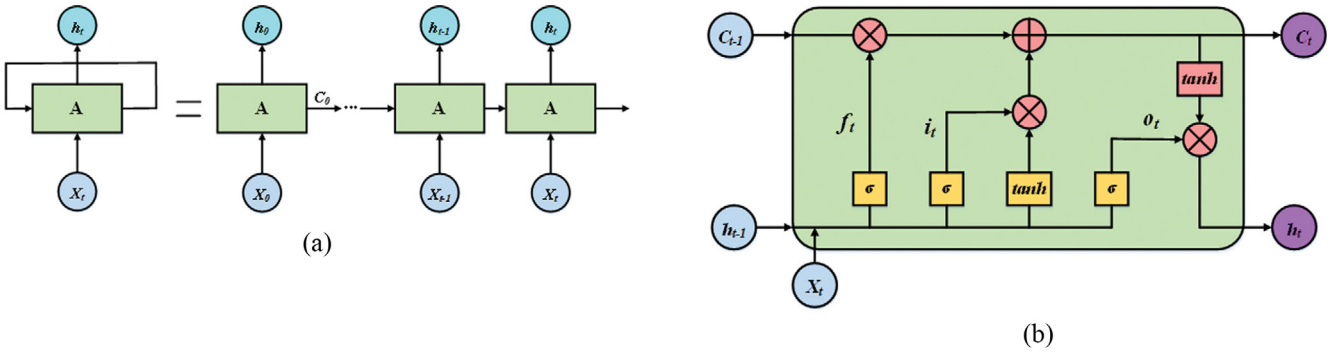

Fig. A1. Principles of LSTM. (a) The structure of RNN. (b) The neural module of LSTM.

APPENDIX B

Figs. B1-2 are the 100-10,100th group of data and the 3,100-13,100th group of data.

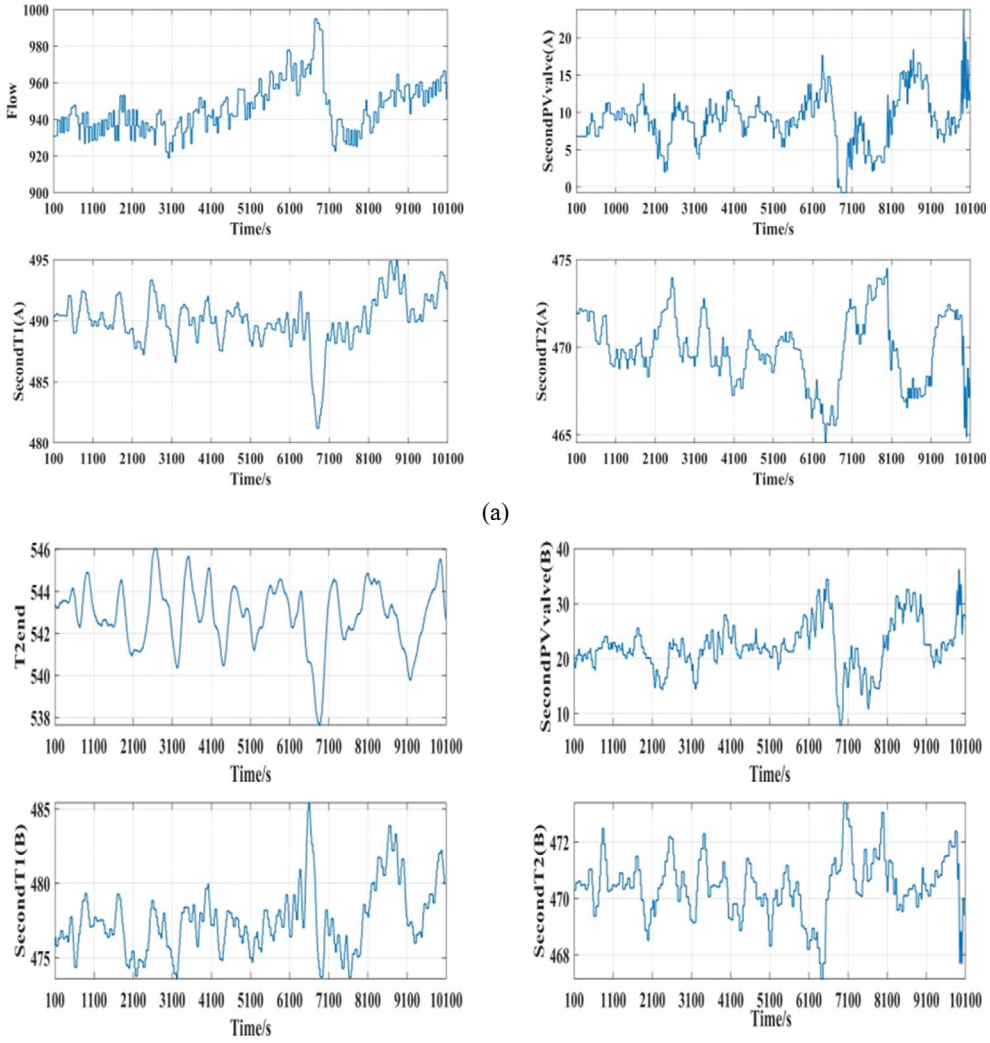

(a)

(b)

Fig. B1. The group of data during the time interval from 100 s to 10,100 s. (a) Total flow and variables at Side A. (b) Superheated steam temperature and variables at Side B.

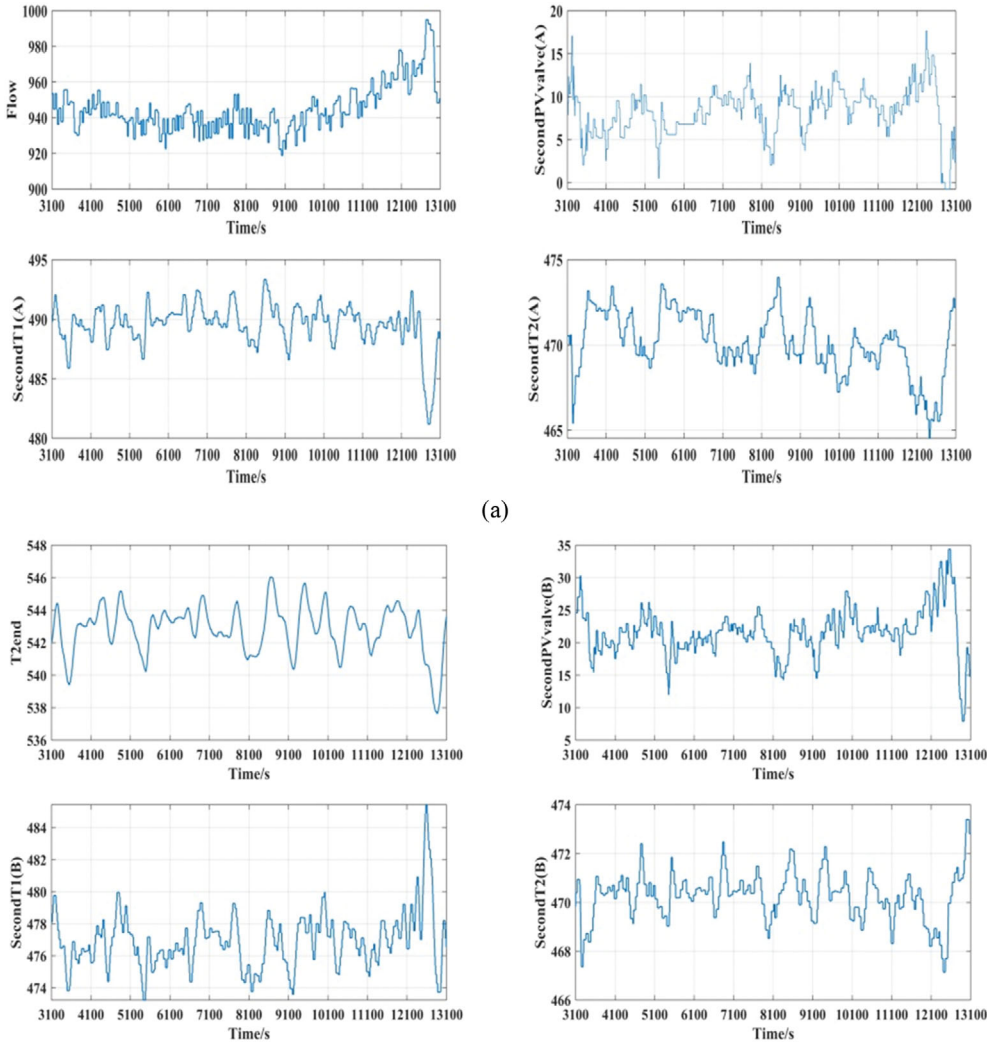

Fig. B2. The group of data during the time interval from 3,100 s to 13,100 s. (a) Total flow and variables at Side A. (b) Superheated steam temperature and variables at Side B.

APPENDIX C

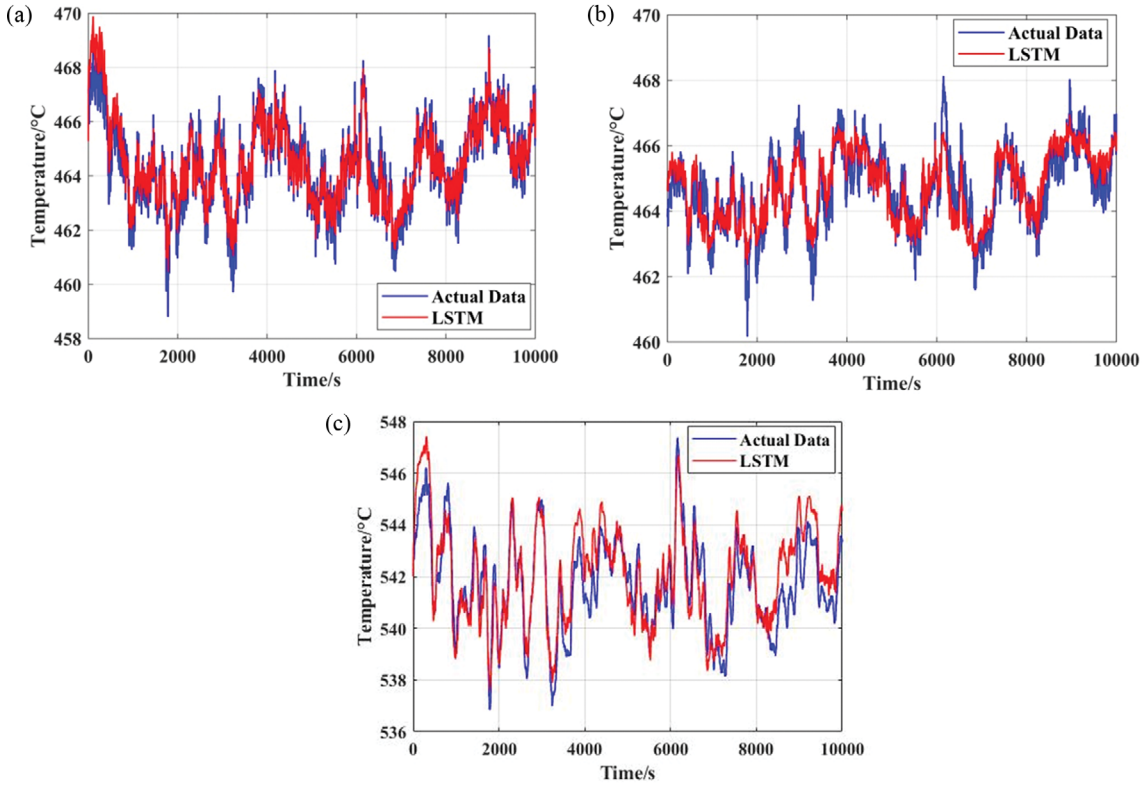

Fig. C1. Model identification based on LSTM. (a) The model of desuperheater at Side A. (b) The model of desuperheater at Side B. (c) The model of secondary superheater.

APPENDIX D

In general, for an *n*-th order process, an (n+1)-th order observer would be needed to estimate disturbances. However, since it is difficult to determine the model order, a low-order ESO is usually preferred in practice [36]. The principal schematic of ESO is shown in Fig. D1, where y is the output, r is the set point, G_p denotes the controlled object, b_0 and k_p are both the parameters to be adjusted, z_3 is the total disturbance.

When G_p is a second-order system with disturbance, the fourth-order expanded state observer is designed as shown below:

$$\begin{aligned} e_1 &= y - z_1 \\ \dot{z}_1 &= z_2 - \beta_1 e_1 \\ \dot{z}_2 &= z_3 - \beta_2 e_1 + b_0 u \\ \dot{z}_3 &= -\beta_3 e_1 \end{aligned} \tag{D1}$$

It was shown [37] that the derivation process of ADRC and y, $\dot{y}$ and total disturbance can be tracked by variables z_1, z_2 and z_3 well, with a reasonable tuning of β_1, β_2 and β_3.

To compensate the expanded state, the feedback is chosen as follows:

$$u = \frac{u_0 - z_3}{b_0} \tag{D2}$$

By combing the variables [38], we can reduce the number of parameters to be tuned as shown below.

$$\beta_1 = 3w_0 \quad \beta_2 = 3w_0^2 \quad \beta_3 = w_0^2 \tag{D3}$$

where w_0 is the system bandwidth.

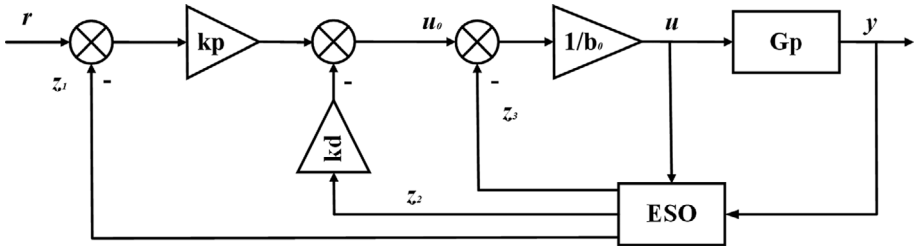

Fig. D1. Principal schematic of ESO.

APPENDIX E

From Fig. E1, the internal model's transfer function can be written as:

$$\phi(s)=\frac{y(s)}{u_0(s)}=\frac{b(s-4w_0)(s+w_0)}{b_0(s^2-3w_0s-3w_0^2)(s^2+a_1s+a_2)+bw_0^2s^2} \quad \text{(E1)}$$

The characteristic equation of the closed-loop system is shown as follows:

$$1+\phi(s)H(s)=0 \quad \text{(E2)}$$

where H(s) is the transfer function of the PID controller.

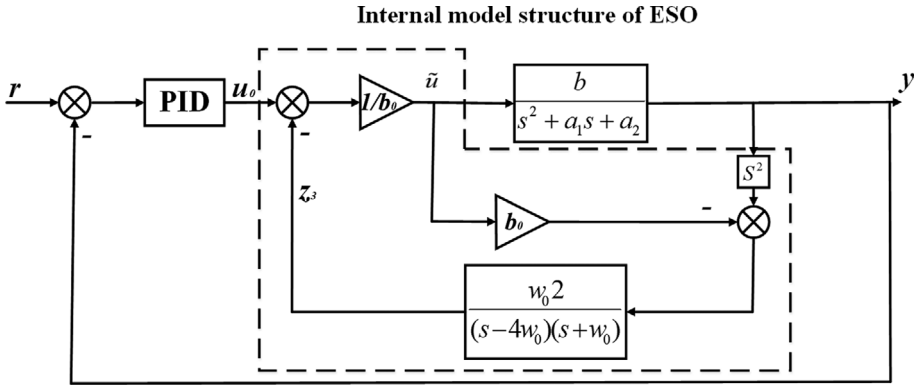

Fig. E1. Structural transformation of ADRC.